ORIGINAL RESEARCH

Ultrasound Molecular Imaging of Neovascularization for Evaluation of Endometrial Receptivity Using Magnetic iRGD-Modified Lipid-Polymer Hybrid Microbubbles

Yanni He[1,]*, Meijun Zhou[1,]*, Sushu Li[1,]*, Zheli Gong[2], Fei Yan[3], Hongmei Liu[1]

[1]Department of Ultrasound, Institute of Ultrasound in Musculoskeletal Sports Medicine, Guangdong Second Provincial General Hospital, Guangzhou, 510317, People's Republic of China; [2]Department of Ultrasound, The People's Hospital of Hunan Province, Changsha, 410061, People's Republic of China; [3]CAS Key Laboratory of Quantitative Engineering Biology, Shenzhen Institute of Synthetic Biology, Shenzhen Institute of Advanced Technology, Chinese Academy of Sciences, Shenzhen, 518055, People's Republic of China

*These authors contributed equally to this work

Correspondence: Hongmei Liu, Department of Ultrasound, Institute of Ultrasound in Musculoskeletal Sports Medicine, Guangdong Second Provincial General Hospital, Guangzhou, 510317, People's Republic of China, Tel/Fax +86-19924270557, Email hongmeiliu3@163.com; Fei Yan, CAS Key Laboratory of Quantitative Engineering Biology, Shenzhen Institute of Synthetic Biology, Shenzhen Institute of Advanced Technology, Chinese Academy of Sciences, Shenzhen, 518055, People's Republic of China, Tel/Fax +86-755-86392284, Email fei.yan@siat.ac.cn

Background: Angiogenesis plays an important role in endometrial receptivity, determining the response of the endometrium to the blastocyst at the early stage of embryo implantation. During the application of assisted reproduction technologies, it is very important to evaluate the status of uterine angiogenesis before deciding on embryo implantation. Targeted microbubbles (MBs)-based ultrasound molecular imaging (UMI) can noninvasively detect the expression status of biomarkers at the molecular level, thereby being a potential diagnosis strategy for various diseases and their therapeutic evaluation.

Methods: The iRGD-lipopeptide (DSPE-PEG2000-iRGD) conjugate was prepared with iRGD peptides and DSPE-PEG2000-maleimide through the Michael-type addition reaction. Then, the magnetic iRGD-modified lipid-polymer hybrid MBs (Mag-iLPMs) were prepared with the double-emulsification-solvent-evaporation method. Magnetic targeting of Mag-iLPMs was confirmed under the microscope, followed by a rectangular magnet. Next, the in vitro targeted binding of MBs to murine brain-derived endothelial cells.3 (bEnd.3) and human umbilical vein endothelial cells (HUVEC) were evaluated. The ratio of MBs binding to bEnd.3 and HUVEC at the same field was also compared. For in vivo studies, bolus injections of targeted or control MBs were randomly administrated to non-pregnant or pregnant rats on day 5. Then, the uteri were imaged using a VisualSonics Vevo 2100 ultrasound system (Fujifilm VisualSonics Inc., Ontario, Canada) equipped with a high-frequency transducer. Ultrasonic imaging signals were acquired from Mag-iLPMs, and compared with Mag-LPMs, iLPMs, and LPMs.

Results: The Mag-iLPMs showed excellent performance in ultrasound contrast imaging and binding affinity to target cells. Using the magnetic field, 10.5- and 12.47-fold higher binding efficiency to bEnd.3 and HUVEC were achieved compared to non-magnetic iLPMs, respectively. Significantly enhanced UMI signals were also observed in the uteri of rats intravenously injected pregnant rats (6.58-fold higher than rats injected with iLPMs).

Conclusion: We provided a powerful ultrasonic molecular functional imaging tool for uterine angiogenesis evaluation before embryonic implantation.

Keywords: endometrial receptivity, ultrasound molecular imaging, $\alpha v \beta_3$ integrin

Introduction

Embryonic implantation is a crucial period of human embryogenesis.[1–3] Up to a third of human embryos can not successfully implant into the endometrium, resulting in spontaneous abortions.[4–7] Generally, successful embryonic

implantation depends on the synchronization between the developing blastocyst and the receptive endometrium.[8] The "implantation window" or endometrial receptivity is spatiotemporally restricted and is only sustained for about 48 h in humans. During the "implantation window", molecular events underlying this process are established. Therefore, evaluating the endometrial receptivity to improve embryo implantation rate in reproductive medicine remains a big challenge.

Several studies have revealed that the pinopodes expressed on the endometrial epithelial cells are the optimum morphological marker to evaluate endometrial receptivity.[9] Developed pinopodes exist only in the "implantation window", 6 to 8 days after ovulation.[10] The appearance, development and degeneration of pinopodes are almost precisely synchronized with the start and the end of the endometrium "implantation window", affecting different stages of embryo implantation.[9] Additionally, pinopodes in the rat endometrium increase on pregnancy day 4, and reach a peak on day 5, then rapidly decrease on day 6.[11,12] Moreover, the expression of $\alpha v\beta_3$ integrin in endometrial pinopodes and blastocyst trophectoderm plays an important role during embryo implantation.[13] Besides, $\alpha v\beta_3$ integrin presents a high expression on activated endothelial cells during angiogenesis, participating in the development of new vessels by elongation and intussusception.[14] Furthermore, endometrial angiogenesis plays an important role in female fertility, including follicular development, periodical endometrial regeneration, embryo implantation, and placentation.[15–17] The vascularity in the endometrium affects endometrial receptivity to the blastocyst during the "implantation window".[18,19] Then, the endometrium grows thicker as the vessel gradually grows mature, implicating sufficient endometrial receptivity for embryo implantation.[19]

Many researchers have studied the endometrial molecular expression in humans via endometrial biopsy during the "implantation window".[20] However, the acquisition of endometrial tissue is traumatic and is not suitable to prepare for the pregnancy period. Ultrasonography (US) is non-invasive and repeatable and is the most common method used to assess endometrial receptivity, including endometrial thickness, and the endometrial and uterine artery blood flow spectrum parameters. Nevertheless, there are no standardized diagnostic criteria for different conventional ultrasonography assessing endometrial receptivity, resulting in doubtable accuracy.[21–24] Moreover, contrast-enhanced ultrasound (CEUS) can be used to predict endometrial receptivity by measuring endometrial and sub endometrial blood flow.[25]

Furthermore, CEUS imaging is a valuable tool for preclinical and clinical diagnostics.[26] The most frequently used ultrasound contrast agents (UCAs) are microbubbles (MBs). The US signal can be further enhanced by UCAs that amplify the detection. Additionally, CEUS techniques using targeted MBs that can adhere to specific biomarkers on cells have been used for ultrasound molecular imaging (UMI), presenting a great potentials to monitor the molecular status. So far, MBs are functionalized with various targeting ligands. Targeted MBs can be used to detect disease-related functional state, such as inflammation and angiogenesis.[27] Many targets related to neo-angiogenesis have been proposed for UMI, including $\alpha v\beta_3$ integrin and vascular endothelial growth factor receptor-2 (VEGFR-2). Thus, UMI is a powerful technique for preclinical diagnosis, studying disease mechanism, and monitoring of therapeutic effects. However, the binding affinity of ligands modified on the surface of MBs might not be enough to resist the high flow shear stress, especially in large blood vessels. Therefore, in the present study, we constructed iRGD-modified lipid-polymer hybrid MBs with magnetic nanoparticles (Mag-iLPMs). We hypothesized that these Mag-iLPMs would enhance the binding affinity and improve UMI for evaluating endometrial receptivity with a magnet-guide.

Materials and Methods
Materials

The 1,2-distearoyl-sn-glycero-3-phosphatidylcholine (DSPC) and 1,2distearoyl-sn-glycero-3-phosphoethanolamine N [methoxy(polyethylene glycol)-2000] (DSPE-PEG2000) were purchased from Avanti Polar Lipids Inc. (Alabaster, AL, USA). Fe_3O_4 nanoparticles (Fe_3O_4-NPs) were purchased from Nanjing Nanoeast Biotech Co., Ltd. Poly(DL-lactide-co-glycolide) (PLGA) (10,000) (50/50) was purchased from Jinan Daigang Biological Material Co., Ltd. Agarose powder, $(NH_4)HCO_3$ and polyvinyl alcohol (PVA) (30–70 kDa) were obtained from Sigma-Aldrich Co., Ltd. iRGD peptide (CRGDKGPDC-NH2) and 5-FAM-iRGD peptide were obtained from Shanghai GL Biochem Co., Ltd. DMEM, penicillin and streptomycin were obtained from HyClone Biochemical Products Co., Ltd. FBS was purchased from

Gibco Co., Ltd. Murine bEnd.3 endothelial cells (bEnd.3) and human umbilical vein endothelial cells (HUVEC) were purchased from the EK-Bioscience Biotechnology Company Limited Shanghai Enzyme Research.

Preparation of Magnetic iRGD-Modified Lipid-Polymer Hybrid Microbubbles (Mag-iLPMs)

The iRGD-lipopeptide (DSPE-PEG2000-iRGD) conjugate was prepared with iRGD peptides and DSPE-PEG2000-maleimide through the Michael-type addition reaction.[28,29] Magnetic nanoparticles (Fe_3O_4-NPs) were dispersed in double distilled water to form a suspension at 2 mg/mL and treated with sonication for 20 min in the pulse mode with (3 s off, 3 s on) to prepare Fe_3O_4-NPs storage solution. Then, the magnetic iRGD-modified lipid-polymer hybrid MBs (Mag-iLPMs) were prepared using the double-emulsification-solvent-evaporation method.[30] Briefly, DSPE-PEG2000-iRGD (1 mg), DSPE-PEG2000 (1.5 mg), and PLGA (50 mg) were dissolved in 1 mL methylene chloride. The above oil phase was added into an water phase composed of 400 μL Fe_3O_4-NPs solution and $(NH_4)HCO_3$ aqueous solution (6% w/v, 200 μL), followed by sonication for 120 s (3 s on, 3 s off). Then, 5 mL 4% w/v of PVA solution was added to the above solution and homogenized using an IKA homogenizer for 5 min at 5000 rpm. The resultant solution and 10 mL of deionized water were mixed and homogenized for another 5 min, then stirred for 4 h to evaporate the organic solvent. Subsequently, Mag-iLPMs were centrifuged at 5000 g for 5 min. The precipitate of Mag-iLPMs was rinsed with deionized water thrice. Finally, Mag-iLPMs were lyophilized for 24 h. Dry sample were stored at 4 °C. The 5-FAM-iRGD-lipopeptide (5-FAM-DSPE-PEG2000-iRGD) was prepared by conjugating 5-FAM-iRGD peptide to DSPE-PEG2000-maleimide through Michael-type addition reaction.[27,28] The fluorescence-labeled Mag-iLPMs were prepared using the same method adding 5-FAM-DSPE-PEG2000-iRGD instead of DSPE-PEG2000-iRGD.

Characterization of Mag-iLPMs

The particle size of LPMs, Mag-LPMs, iLPMs, and Mag-iLPMs were measured using Nano Measurer software by analyzing three different scanning electron microscope (SEM) images. The surface morphology of Mag-iLPMs was observed with a scanning electron microscope (SEM) (JEOL Technics, Tokyo, Japan). The magnetic particles and shape of Mag-iLPMs were observed with a transmission electron microscope (TEM) (JEOL JEM-1400). The content of Fe in Mag-iLPMs was determined using Agilent 720ES ICP-OES (PerkinElmer, Massachusetts, USA). The Mag-iLPMs synthesized with PLGA and 5-FAM-DSPE-PEG2000-iRGD were observed with a fluorescent microscope (Olympus IX71, Japan) to evaluate the combination of iRGD-lipopeptide and the polymer. Fluorescent MBs were also observed with a fluorescent microscope (Leica DMI3009B, Wetzlar, Germany).

CEUS Imaging of Mag-iLPMs in vitro

The CEUS imaging of Mag-iLPMs in vitro was performed on a phantom of agarose (3% w/v). Mag-iLPMs with different concentrations (0.625, 1.25, 2.5, 5 and 10 mg/mL) were added into the phantom holes. A VisualSonics Vevo 2100 ultrasound system equipped with MS250 linear array transducer was used for CEUS. The parameters were set to 18.0 MHz harmonic frequency, 35 dB dynamic range and 4% transmit power.

Evaluation of Magnetic Targeting and CEUS of Mag-iLPMs in vitro

First, 1 mg/mL Mag-iLPMs was dropped into a 10 cm petri dish, then placed under the microscope, followed by placing a rectangular magnet close to the petri dish to record the magnetic attraction process. A phantom with lumen was used to observe the movement of the Mag-iLPMs in vitro under the influence of the magnetic field using CEUS. Rectangular magnets with different magnetic field intensities were put at the bottom of the phantom, and 1 mg/mL Mag-iLPMs was injected into the lumen. Then, the magnetic attraction process was recorded. 4 min after injection of Mag-iLPMs, the echo signal intensity was measured in the lumen under the magnetic field.

Cell Culture and in vitro Targeted Binding Experiment

The bEnd.3 and HUVEC were cultured in a 6-well plate (1×10^5 cells per well) for overnight using DMEM (Hyclone) mixed with 10% FBS (Gibco), 100 IU/mL penicillin (Hyclone) and 100 μg/mL streptomycin (Hyclone), maintaining at 37 °C, 20% O_2, 5% CO_2 and humidified conditions. Then, the static binding of αvβ₃ integrin-targeted LPMs to cells was performed. 1 mL of 5-FAM-labeled LPMs, 5-FAM-labeled Mag-LPMs, 5-FAM-labeled iLPMs or 5-FAM-labeled Mag-iLPMs were added into the cell monolayer and rectangular magnets were positioned under the plates. The cell culture plates were sealed and rotated on the shaking table for 4 min. Next, rectangular magnets were removed and free MBs were washed away using PBS. The number of MBs targeted binding to cells was counted under a fluorescent microscope (Olympus, Tokyo, Japan) at five random fields of view. The ratio of MBs binding to cells in the same field of view was used to assess their attachment capability.

Ultrasound Imaging and in vitro Adhesion Experiment

The HUVEC were cultured in a 10 cm petri dish (8×10^5 cells per well) for overnight in DMEM mixed with 10% FBS and 1% penicillin-streptomycin solution at 37 °C, 20% O_2, 5% CO_2, and humidified conditions.Then, the static binding of αvβ₃ integrin-targeted Mag-iLPMs to cells was performed. First, 1 mL of Mag-iLPMs was added into the cell monolayer and rectangular magnets were positioned under the plate. The cell culture plates were sealed and rotated on the shaking table for 4 min. Next, the rectangular magnets were removed and free Mag-iLPMs were washed away using PBS. The cells were digested, centrifuged and resuspended with DMEM complete medium. The HUVEC cultured in a 10 cm petri dish with the same cell density and Mag-iLPMs dissolved in the DMEM complete medium with the same concentration were used as the contrast groups.

Animals

First, female and male SD rats (8–10 weeks) were bred in estrus. Pregnancy day 1 was determined when the vaginal plugging appeared in female rats. Both non-pregnant and pregnant rats were included in this study. Considering the double uteri of female rat, the left uterus was imaged. Since the "implantation window" of rats occurs on pregnancy day 5 and is considered the highest endometrial receptivity, bolus injections of targeted or control MBs were randomly administrated on non-pregnant or pregnant rats on day 5. All rats underwent UMI around at 18:00. Briefly, rectangular magnets were placed on the uteri of non-pregnant or pregnant rats and the prepared 1 mL of LPMs, Mag-LPMs, iLPMs, or Mag-iLPMs (5 mg/mL) was intravenously injected, respectively. Rectangular magnets were removed 4 min after injection. And 1 mL of Mag-LPMs or Mag-iLPMs (5 mg/mL) was intravenously injected into pregnant rats without magnet-guide. Blood was collected before and after injections for routine blood tests, including red blood cell counts, platelet counts, and white blood cell counts. The health of rats was monitored for 2 h after UMI. Then, the female rats were sacrificed and the embryos were confirmed.[27] The main organs resected were fixed, paraffin-embedded and sliced. Next, H&E staining of the resected main organs and blood analysis was used to evaluate the safety of MBs. All animal experiments were performed under the guidelines for ethical review of laboratory animal welfare (GB/T 35892–2018) and were approved by the Animal Study Committee of Shenzhen Institutes of Advanced Technology, Chinese Academy of Sciences.

Statistical Analyses

SPSS 20.0 (IBMCorp, Armonk, New York, USA) was used to process the data. The data were expressed as means ± s.d. After determining the homogeneity of variance in the measurement data, t-tests were performed. The Mann–Whitney test was used for counting data. A $p < 0.05$ was considered statistically significant.

Results

Preparation and Characterization of Mag-iLPMs

The Mag-iLPMs were successfully prepared using the double-emulsification-solvent-evaporation method (Figure 1A). The bright-field image of the targeted Mag-iLPMs under the optical microscope showed a spherical appearance (Figure S1). The
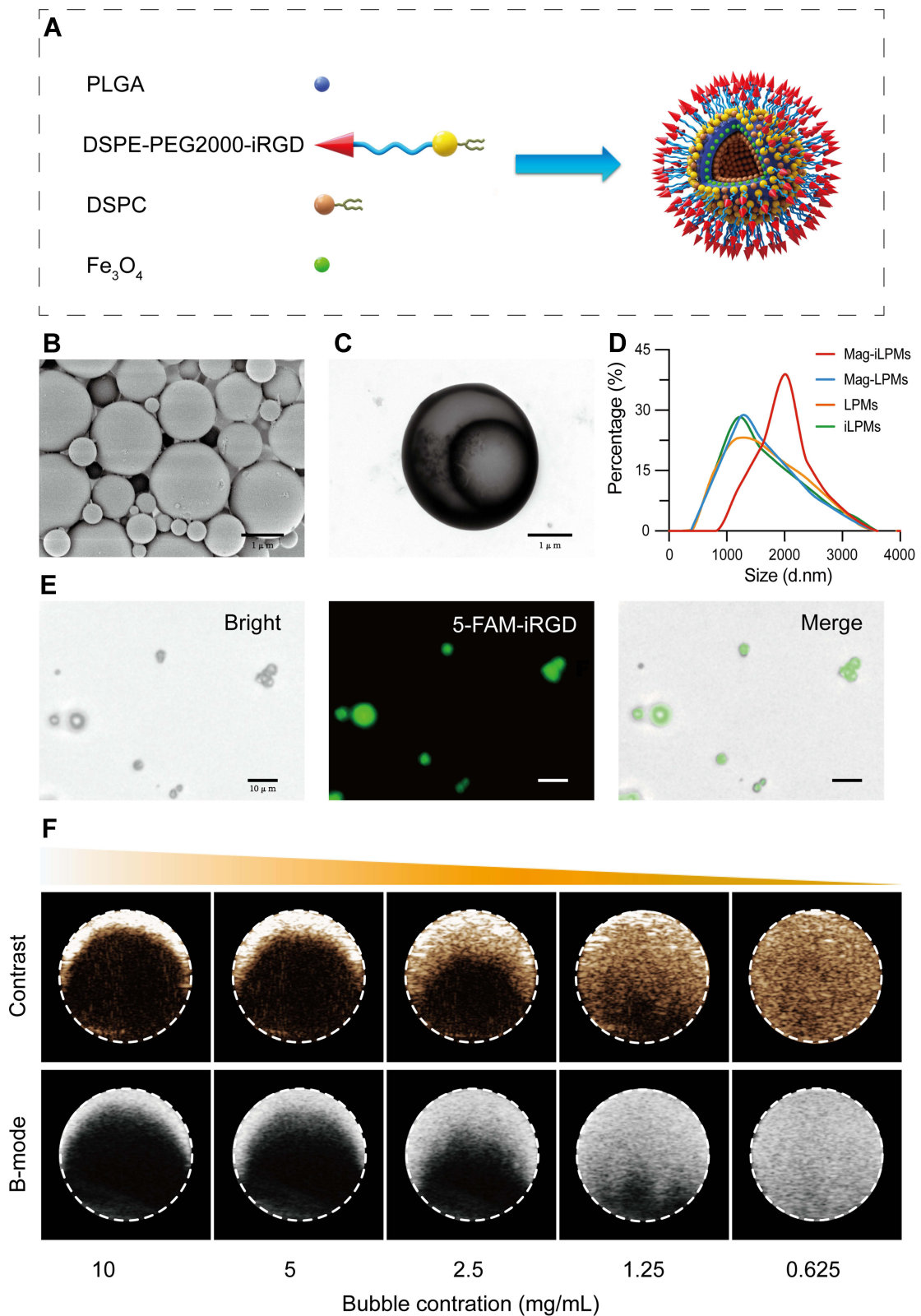
Figure 1 Synthesis and characterization of Mag-iLPMs. (**A**) Schematic illustration of the preparation of Mag-iLPMs. (**B**) SEM of Mag-iLPMs. Scale bar = 1 μm. (**C**) TEM of Mag-iLPMs. Scale bar = 1 μm. (**D**) Typical size distribution of LPMs, Mag-LPMs, iLPMs and Mag-iLPMs. (**E**) Fluorescence microscopic images of Mag-iLPMs show the presence of 5-FAM-iRGD (green) on the bubble shell. Scale bar = 10 μm. (**F**) Ultrasound images of Mag-iLPMs in vitro at different concentrations in B-mode and nonlinear contrast mode.

Mag-iLPMs also exhibited a spherical appearance in the SEM (Figure 1B). The TEM images showed that the Mag-iLPMs presented a hollow structure, with many black nanoparticles encapsulated in the shell (Figure 1C). The typical size distribution of LPMs, iLPMs, Mag-LPMs and Mag-iLPMs are illustrated in Figure 1D. The mean size of LPMs, iLPMs, and Mag-LPMs was 1518.00 ± 729.30, 1549.00 ± 769.2, 1627.00 ± 977.00 nm, respectively (Figure S2). However, the mean size of Mag-iLPMs increased to 1862.00 ± 674.90 nm (Figure S2). The particle size of Mag-iLPMs lyophilized powder did not significantly change after 15 days of storage (Figure S3). The Fe loading of Mag-iLPMs reached 0.44 wt%, and weight percentage of Fe_3O_4 was 0.61 wt%. The fluorescence micrographs showed that Mag-iLPMs emitted green fluorescence (5-FAM-DSPE-PEG2000-iRGD) from bubble shells, revealing the iRGD peptide coating on the shell (Figure 1E). Mag-iLPMs emitted red (DiI-labeled PLGA) and green (5-FAM-DSPE-PEG2000-iRGD) fluorescence from bubble shells in Figure S4, revealing uniform hybridization of polymers and lipids on the shell. To investigate the echo intensity of Mag-iLPMs, different concentrations of Mag-iLPMs were poured into holes of the phantom for CEUS with a dual-display (B-mode and contrast mode). The acoustic signals weakened with decreased concentrations of Mag-iLPMs (Figure 1F). Overall, the excellent imaging capability of Mag-iLPMs demonstrated that they can be used as UCAs for CEUS.

Validation of the Magnetic Responsiveness of Mag-iLPMs

To test whether Mag-iLPMs have the magnet-targeted ability, we evaluated the magnet targeting and responsiveness of Mag-iLPMs. The Mag-iLPMs moved directionally towards the magnet with magnetic guidance (Figure 2A and Video 1). Without the magnetic field, the Mag-iLPMs injected into the tube flowed along with the pushing direction. Upon exposure to the magnetic field, the Mag-iLPMs moved backwards to the magnetic field and were retained, which could be observed by ultrasonography in the contrast mode (Figure 2B and Video 2). Additionally, the targeted imaging ability was enhanced with stronger magnetic fields, and was steady with magnetic field intensities higher than 2000 Gs (Figure S4). Similarly, when
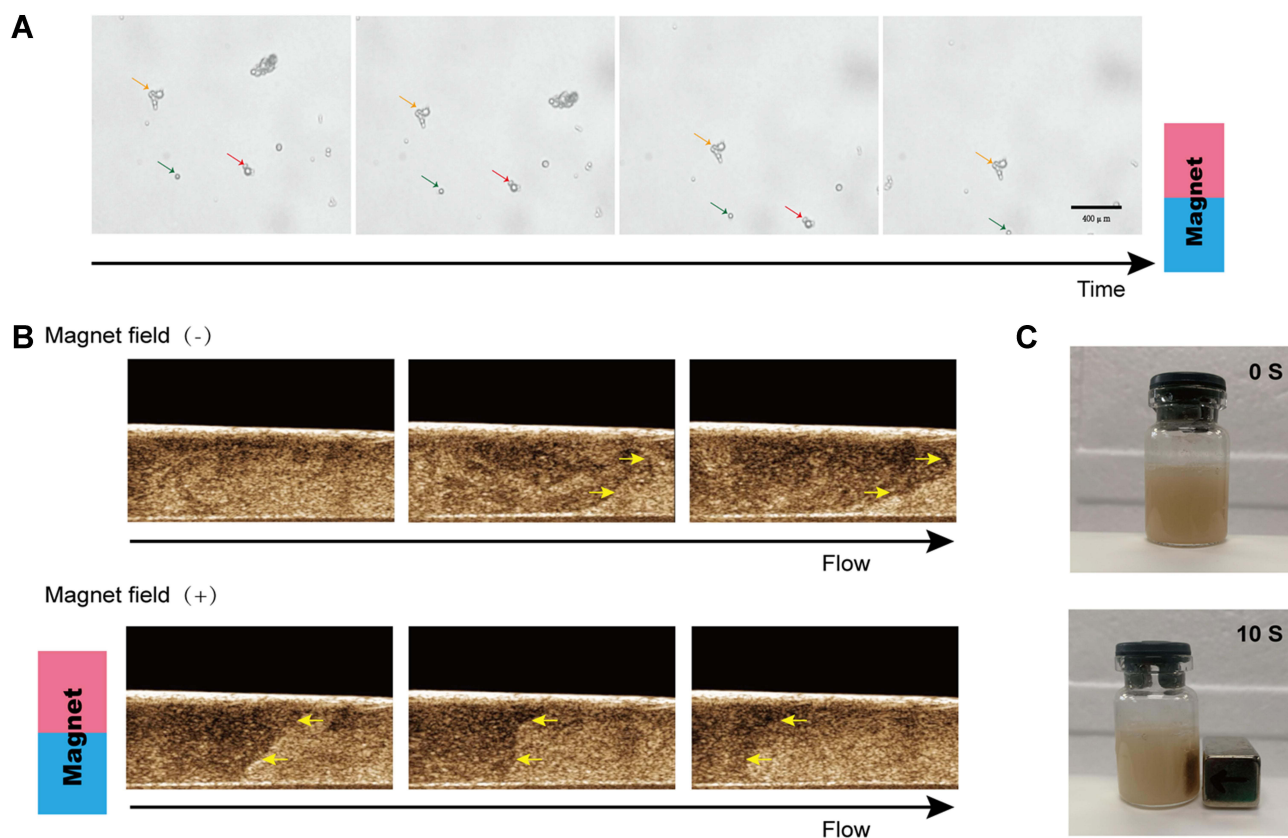
Figure 2 Magnetic attraction assay of Mag-iLPMs in vitro. (**A**) Optical images of Mag-iLPMs dispersed in water. Scale bar = 400 μm. (**B**) Ultrasound images of Mag-iLPMs injected into the transparent lumen mimicking vessel without or with a magnet. (**C**) Photographs of Mag-iLPMs dispersed in water before and 10s after the application of the magnetic field.

Mag-iLPMs were dispersed in water in an ampere bottle with a magnet placed at one side, Mag-iLPMs could move towards the side with a magnet within 10s (Figure 2C).

Examination of $\alpha v \beta_3$ Integrin-Targeted Mag-iLPMs Binding Efficiency to bEnd.3 and HUVEC

The fluorescence micrography images of 5-FAM-labeled LPMs, iLPMs, Mag-LPMs, and Mag-iLPMs (green) binding to bEnd.3 under magnetic fields are presented in Figure 3A. A large number of Mag-iLPMs were attached to bEnd.3 with magnetic guidance under the optical microscope (Figure 3A). The quantitative analysis showed that the Mag-iLPMs targeted adhesion to bEnd.3 was significantly higher than LPMs, iLPMs or Mag-LPMs with magnet-guide (LPMs = 0, iLPMs = 18 ± 15, Mag-LPMs = 28 ± 7, Mag-iLPMs = 189 ± 36, ****$p < 0.0001$; Figure 3B). Moreover, the binding affinity to bEnd.3 of Mag-iLPMs increased with the addition of DSPE-PEG2000-iRGD (Figures S6 and S7). Fluorescence micrographs of 5-FAM-labeled LPMs are presented in Figure 3A and S8. iLPMs (green) binding to HUVEC was also observed. The merged image showed that iLPMs could adhere to the surface of HUVEC while LPMs were scattered in the intercellular space. Additionally, the Mag-iLPMs targeted adhesion to HUVEC were significantly higher than LPMs, iLPMs or Mag-LPMs with magnet-guide (LPMs = 0 ± 0, iLPMs = 17 ± 18, Mag-LPMs = 38 ± 2, Mag-iLPMs = 212 ± 41, ****$p < 0.0001$; Figure 3C). Finally, the binding affinity of Mag-iLPMs to HUVEC increased with increasing weight ratios of DSPE-PEG2000-iRGD and DSPC (Figures S9 and S10). When the weight ratio of DSPE-PEG2000-iRGD and DSPC was 1.5:1, the binding efficiency of Mag-iLPMs to HUVEC was strongest.

Ultrasound Molecular Imaging in vitro

To evaluate the targeted adhesion of Mag-iLPMs and ultrasonic imaging ability in vitro, the Mag-iLPMs were incubated with HUVEC for 4 min. The cells were digested, centrifuged, washed, and resuspended (Figure 4A). The cells suspensions were imaged with CEUS. The ultrasonic imaging ability was comparable to the same concentration Mag-iLPMs. Significantly stronger ultrasonic signals were detected for HUVEC bound to Mag-iLPMs compared to HUVEC without adhesion of Mag-iLPMs (Figure 4B). The quantitative analysis showed that echo signal intensities (ESI) of HUVEC bound with Mag-iLPMs were higher than without adhesion (HUVEC = 26.98 ± 1.65, Mag-iLPMs+HUVEC = 348.73 ± 96.07, Mag-iLPMs = 307.78 ± 17.56; Figure 4C).

Ultrasound Molecular Imaging in vivo

Female rats have double uteri with a "Y" shape. The ultrasonography showed the transverse section of the two uterine bodies or cervix and the long axis of one uterus (Figure S11). The in vivo targeted and imaging ability of Mag-iLPMs was confirmed by UMI in female rats during the "implantation window". 1 mL MBs were intravenously injected and the rectangular magnets were placed on the skin above the rats' uteri (Figure 4D). Then, the UMI was performed. The rectangular magnets were removed 4 min after injection and the imaging signal was compared. The imaging signal of the uteri of pregnant rats was the highest under the magnetic field using Mag-iLPMs as UCAs, while no imaging signal was detected using LPMs (Figure 4E and Video 3). The ESI of uteri of pregnant rats that received Mag-iLPMs was much higher under the magnetic field than in the other groups (LPMs = 12.81 ± 2.42, Mag-LPMs = 26.82 ± 1.27, iLPMs = 56.41 ± 7.94, Mag-iLPMs = 84.29 ± 7.01), with 6.58-fold higher than rats that received LPMs (Figure 4F). Additionally, without magnetic guidance, the imaging signal of the uteri of pregnant rats decreased using Mag-iLPMs or Mag-LPMs as UCAs (Mag-LPMs = 14.03 ± 2.33 a.u., Mag-iLPMs = 55.47 ± 6.47 a.u.; Figure S12). Meanwhile, scarcely imaging signal could be seen in non-pregnant rats with UMI using either MBs under a magnetic field (Figure S13).

Biological Safety

The safety of LPMs, iLPMs, Mag-LPMs and Mag-iLPMs was evaluated by health monitor for 2 hours after UMI. No obvious complications of abnormal heartbeat and respiration were detected in rats and they returned to normal activities after UMI. Besides, no significant changes were detected in the blood analysis for these rats after treatment with MBs, including red blood cell count, platelet count, and white blood cell count (Figure S14). Additionally, no appreciable
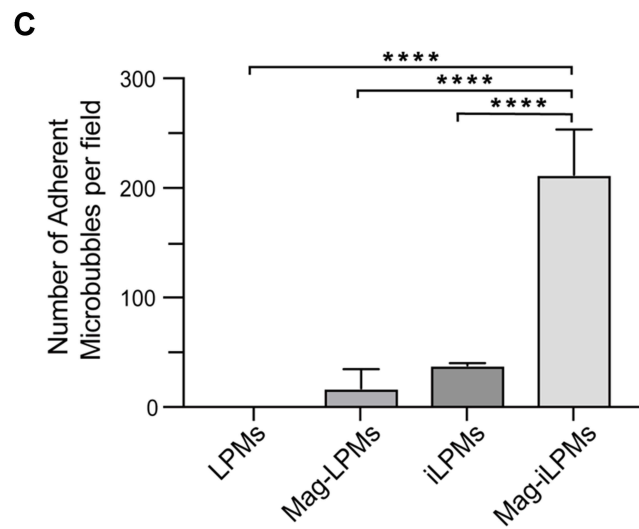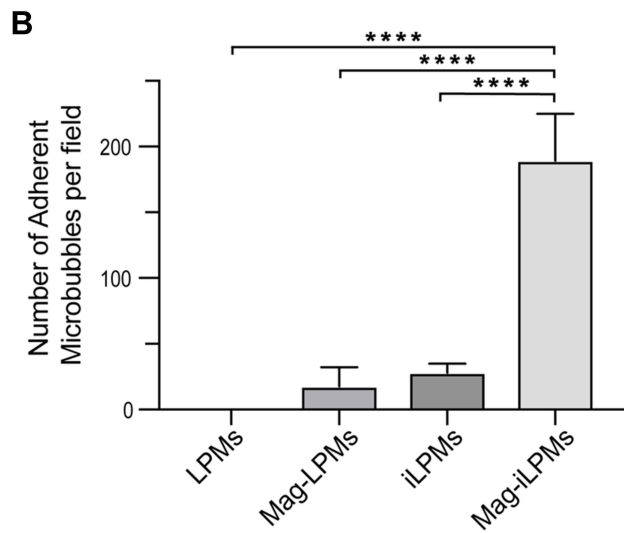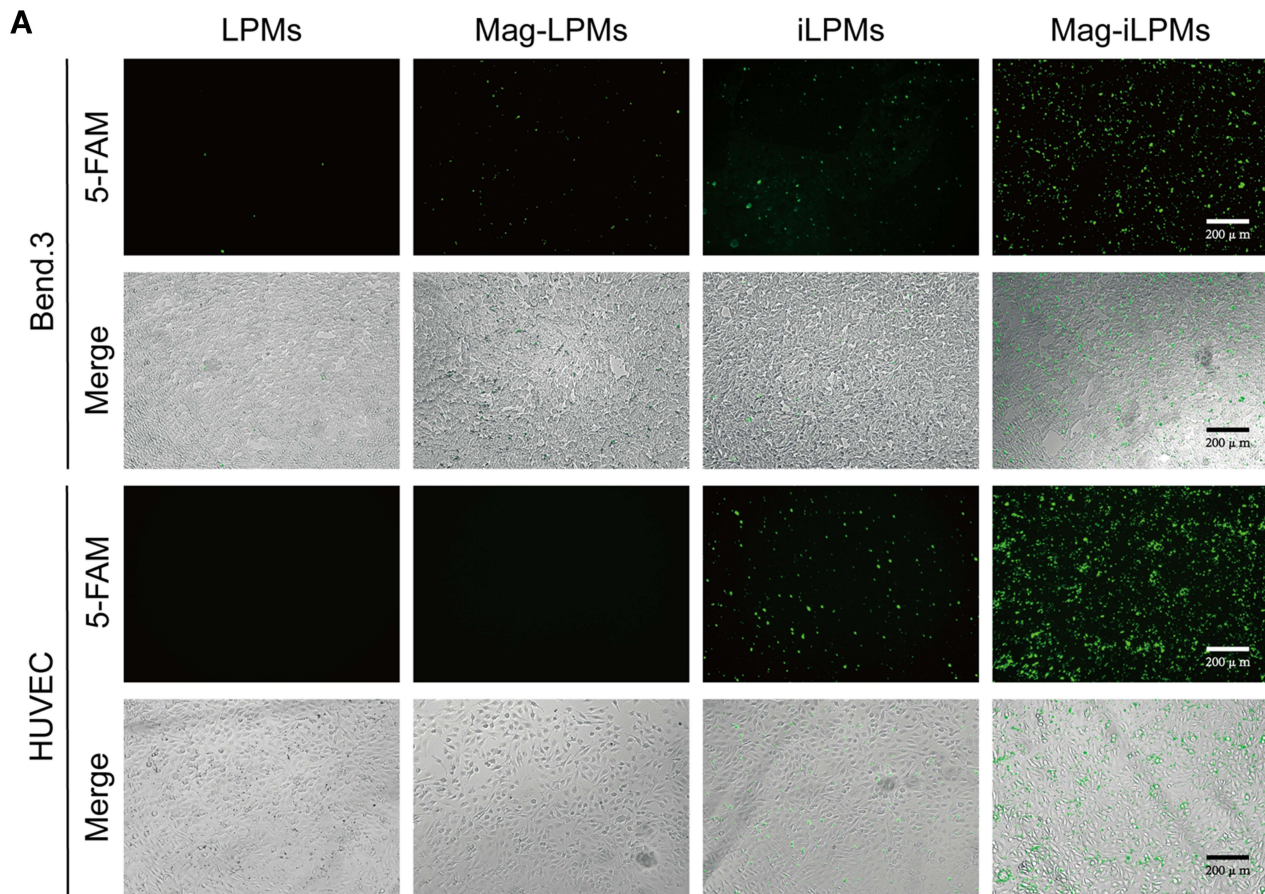
Figure 3 Adhesion of LPMs, Mag-LPMs, iLPMs and Mag-iLPMs to bEnd.3 and HUVEC in vitro. (**A**) Representative fluorescence and merge micrographs for 5-FAM-labeled LPMs, Mag-LPMs, iLPMs and Mag-iLPMs adhered to bEnd.3 and HUVEC. Scale bar = 200 μm. (**B**) Quantitative assay of the number of bEnd.3 adhered to LPMs, Mag-LPMs, iLPMs and Mag-iLPMs from five random view fields. (**C**) Quantitative assay of the number of HUVEC adhered to LPMs, Mag-LPMs, iLPMs, and Mag-iLPMs from five at random view fields. ****$p < 0.0001$.
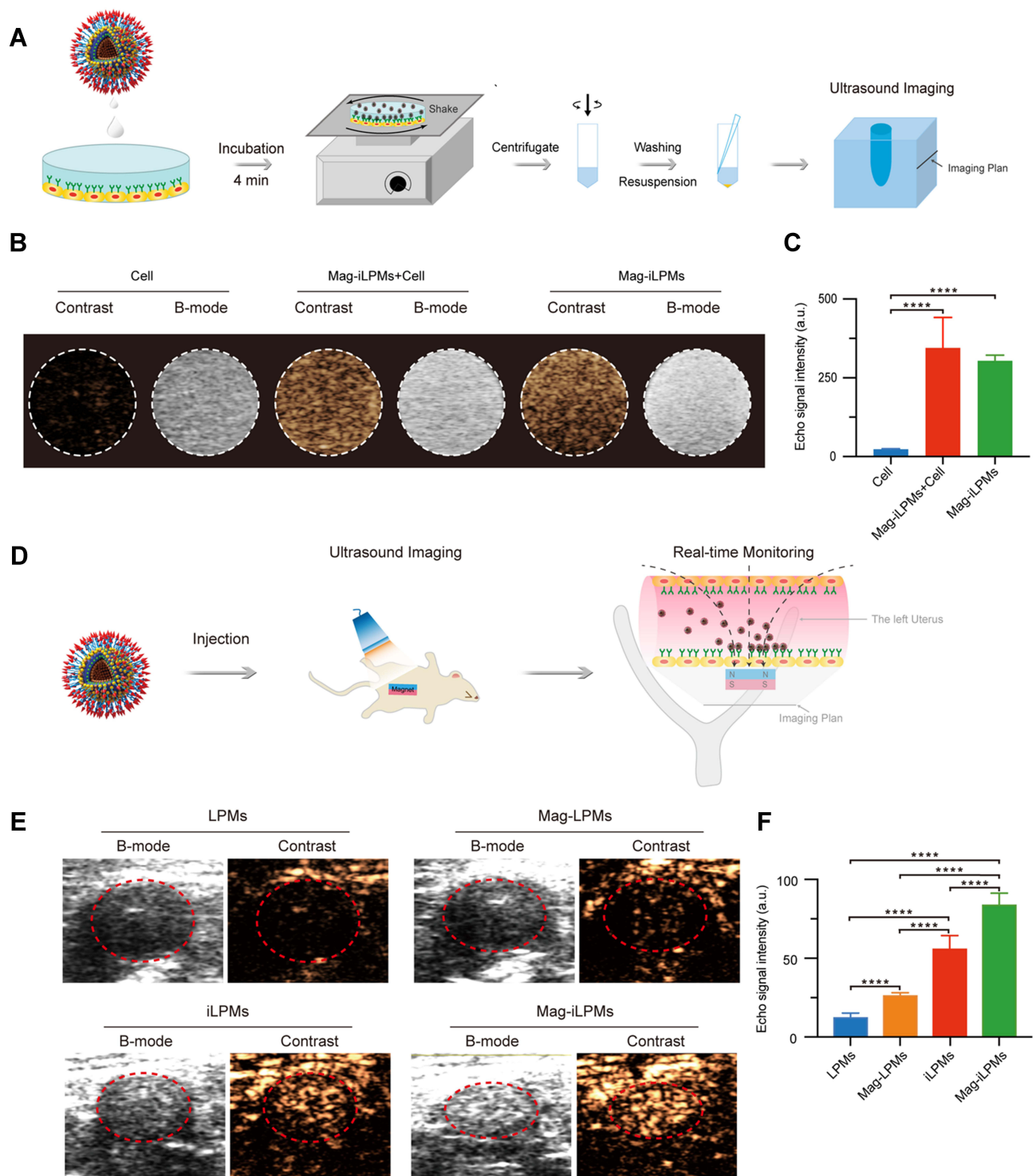
Figure 4 Targeting and ultrasound tracking of Mag-iLPMs. (**A**) Schematic illustration of targeting and ultrasound tracking of Mag-iLPMs in vitro. (**B**) Ultrasound image of HUVEC, Mag-iLPMs and Mag-iLPMs-binding HUVEC in B-mode and nonlinear contrast mode in vitro. (**C**) Quantitative assay for echo signal intensity of HUVEC, Mag-iLPMs and Mag-iLPMs-binding HUVEC. (**D**) Schematic illustration of targeting and ultrasound tracking of Mag-iLPMs in vivo. (**E**) Ultrasound tracking of LPMs, Mag-LPMs, iLPMs and Mag-iLPMs in the uteri of pregnant rats under a magnetic field. (**F**) Quantitative assay for echo signal intensity of the uteri of pregnant rats under a magnetic field. ****$p <$ 0.0001.

abnormality was observed during the histological analysis of the main organs from rats treated with different methods (Figure 5). Altogether, these results demonstrated that the Mag-iLPMs were tolerable and had no obvious acute toxicity in the rats.

Discussion

The synchronized crosstalk between a receptive endometrium and a functional blastocyst is critical for successful implantation.[31] This is the time when embryos penetrate and invade the endometrium, which is called the "implantation window".[32] Thus, optimal endometrial preparation and identification of the "implantation window" for embryo transfer are of great importance. During this process, angiogenesis in the endometrium plays an important role, especially for mother-fetal nutrient and oxygen transport.[34] Therefore, assessing angiogenesis in the endometrium is crucial in evaluating endometrial receptivity. Different methods, such as endometrial biopsy, biologically or biochemical molecular examination, and ultrasonography have been studied to assess endometrial receptivity.[22] Most of them are traumatic or without standardized diagnostic criteria which make them unwelcome in clinical practice.[35] Nevertheless, ultrasound is
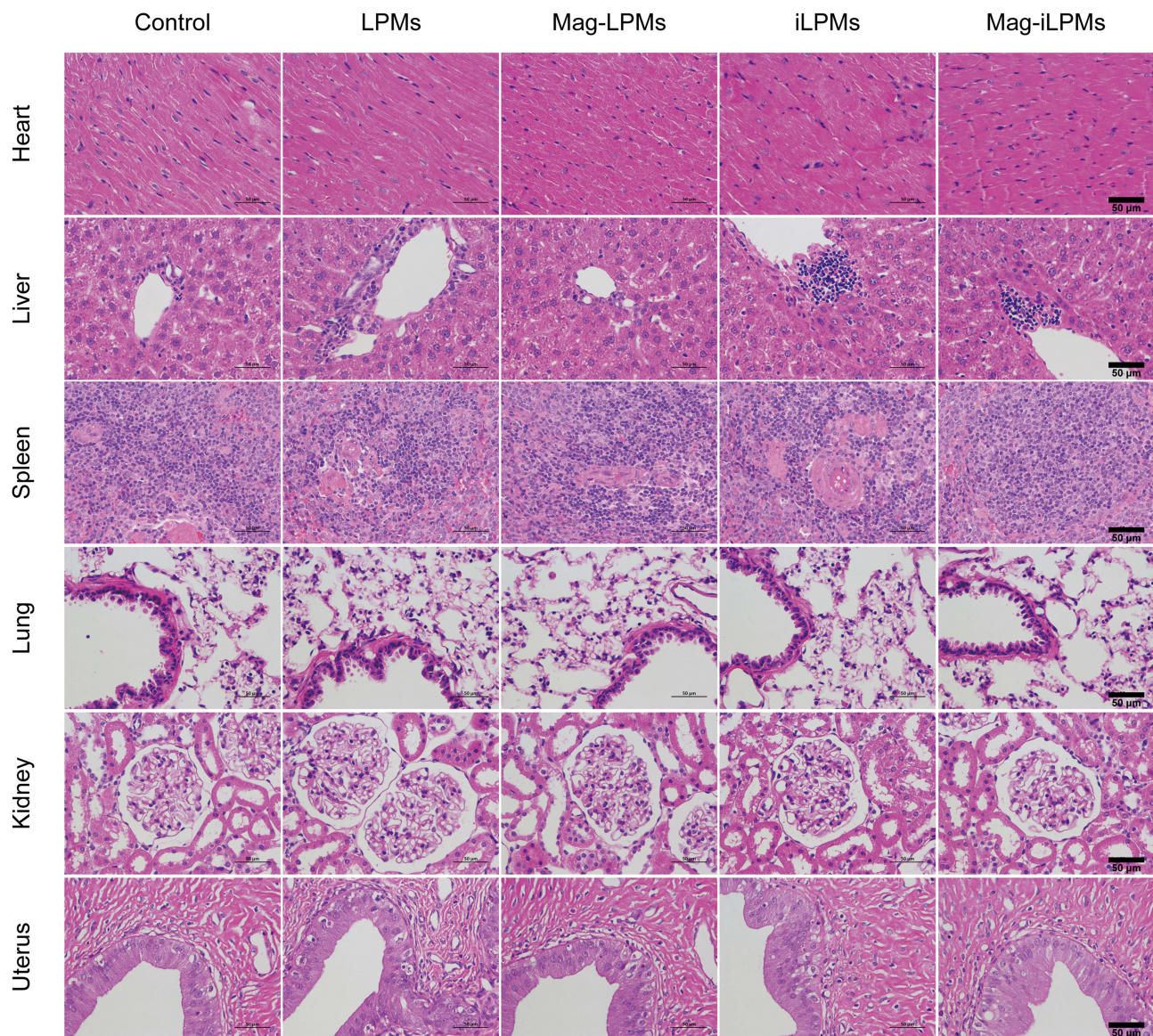
Figure 5 H&E staining of rats' main organs. No significant histological morphological and pathological changes were observed in the main organs (heart, liver, spleen, lung and kidney) of rats in each group. Scale bar = 50 μm.

a common imaging modality in clinics and is safe, non-invasive, real-time and cost-effective. Moreover, UMI combines CEUS with novel molecularly-targeted UCAs, providing a promising strategy for noninvasively assessing biomolecular processes at the molecular level noninvasively.

To perform effective UMI, the selection of molecular targets is crucial. The integrin expressed on the surface of newly formed vascular endothelial cells has different neovascularization from native vessels. The $\alpha v \beta_3$ integrin is highly expressed on activated endothelial cells during angiogenesis. Thus, the targeted detection of $\alpha v \beta_3$ integrin expression in the uterus can reflect uterine angiogenesis. Besides, magnetic targeting can be used to enrich magnetic drug carriers and avoid the rapid clearance of drugs from the targeted region with a magnet guide. Moreover, CEUS is a widely adopted strategy by researchers and clinicians since it is simple and compatible with clinical settings.[33] CEUS techniques using targeted MBs have been used for UMI in different fundamental research, and it offers potential clinical benefits. Therefore, the UMI based on $\alpha v \beta_3$ integrin-targeted magnetic MBs has great potential to assess angiogenesis in the endometrium. In the present study, the in vivo animal experiments demonstrated that UMI is an effective method for noninvasively assessing uterine morphology and molecular pathophysiology.

Here, we synthesized a new type of lipid/PLGA hybrid magnetic MBs decorated with iRGD (Mag-iLPMs) (Figure 1A). The size of the MBs was enlarged with the decoration of Fe_3O_4 magnetic nanoparticles. The Mag-iLPMs had a good contrast imaging capability, and the ultrasound signal intensities enhanced with the concentrations (Figure 1F). It was reported that the appropriate amount of lipid can improve the elasticity of bubble shells, which might improve the harmonic signals and contrast imaging capability of lipid/PLGA MBs.[36] Besides, we demonstrated that Mag-iLPMs have a good magnetic responsive ability (Figure 2). Under magnetic fields, Mag-iLPMs can be enriched in the lumen towards the site of an external magnet. Moreover, their targeting imaging ability was enhanced with stronger magnetic fields (Figure S5). Hence, the ultrasonic imaging signal can be enhanced due to the enhanced interaction between blood vascular endothelial cells and Mag-iLPMs.

To assess the angiogenesis in the endometrium, we decorated MBs with iRGD polypeptide to target $\alpha v \beta_3$ integrin. It can control the permeability of cells, regulate cell internalization and exosmosis, promote deep tissue penetration, and improve imaging sensitivity and therapeutic effect. These effects might be mediated by NRP-1 binding, which the expression increases during proliferation. It might also be involved in hormone-regulated changes in endometrial angiogenesis, preparing the endometrium for implantation.[37] Our current results from cell affinity experiments showed that the MBs decorated with iRGD could specially bind to bEnd.3 or HUVEC (iLPMs bound to bEnd.3 = 18 ± 15, iLPMs bound to HUVEC = 17 ± 18).

Moreover, compared with iLPMs, the magnetic targeting significantly improved the accumulation of Mag-iLPMs in bEnd.3 or HUVEC under magnetic fields (Figure 3). The Mag-iLPMs binding to bEnd.3 and HUVEC were 10.5-, and 12.47-fold more than that of iLPMs, respectively. Thus, as previously reported, magnetic targeting can be controlled to actively gather at the target site with external magnetic fields, thereby potentially increasing the curative effect dose and avoiding many of the disadvantages of systemic administration.[38,39]

Besides, the HUVEC bound with Mag-iLPMs could be visualized by US imaging, and the ESI was 12.93-fold higher than HUVEC before treatment. The ESI in the endometrium of pregnant female rats that received Mag-iLPMs under magnetic field was much higher than those that received Mag-LPMs, iLPMs or LPMs. Meanwhile, without magnetic guidance, the ESI in the endometrium of pregnant female rats with Mag-iLPMs or Mag-LPMs decreased. These results demonstrated the targeted ability of Mag-iLPMs in UMI in vivo under a magnetic field. Moreover, scarcely imaging signal was detected in non-pregnant rats with UMI using either MBs under magnetic field, which suggesting insufficient angiogenesis in the endometrium. Thus, Mag-iLPMs presented a great value to assess the angiogenesis in the endometrium and evaluating endometrial receptivity. Additionally, the health monitor, blood analysis and histological results showed that the resulting MBs were not toxic to major organs in those rats.

In summary, we showed that Mag-iLPMs can be used to improve UMI for the evaluation of $\alpha v \beta_3$ integrin expression on uterine vascular endothelium before implantation. This imaging modality paves the way for its use in clinics for evaluating endometrial receptivity.

Acknowledgments

Disclosure

The authors report no conflicts of interest in this work.

References

1. Aplin JD, Ruane PT, Ewald A. Embryo-epithelium interactions during implantation at a glance. *Cell Sci*. 2017;130:15–22. doi:10.1242/jcs.175943
2. Yu L, Wei Y, Duan J, et al. Blastocyst-like structures generated from human pluripotent stem cells. *Nature*. 2021;591:620–626. doi:10.1038/s41586-021-03356-y
3. Xiang RL, Yin Y, Zheng Y, et al. A developmental landscape of 3D-cultured human pre-gastrulation embryos. *Nature*. 2020;577:537–542. doi:10.1038/s41586-019-1875-y
4. Rimmer MP, Fishwick K, Henderson I, et al. Quantifying CD138+ cells in the endometrium to assess chronic endometritis in women at risk of recurrent pregnancy loss: a prospective cohort study and rapid review. *J Obstet Gynaecol Res*. 2021;47:2149–2156. doi:10.1111/jog.14585
5. Craciunas L, Gallos I, Chu J, et al. Conventional and modern markers of endometrial receptivity: a systematic review and meta-analysis. *Hum Reprod Update*. 2019;25:202–223. doi:10.1093/humupd/dmy044
6. Xin Q, Kong S, Yan J, et al. Polycomb subunit BMI1 determines uterine progesterone responsiveness essential for normal embryo implantation. *J Clin Invest*. 2018;128:175–189. doi:10.1172/JCI92862
7. Franasiak JM, Forman EJ, Hong KH, et al. The nature of aneuploidy with increasing age of the female partner: a review of 15 169 consecutive trophectoderm biopsies evaluated with comprehensive chromosomal screening. *Fertil Steril*. 2014;101:656–663. doi:10.1016/j.fertnstert.2013.11.004
8. Lucas ES, Dyer NP, Fishwick K, et al. Success after failure: the role of endometrial stem cells in recurrent miscarriage. *Reproduction*. 2016;152:R159–R166. doi:10.1530/REP-16-0306
9. Jin XY, Zhao LJ, Luo DH, et al. Pinopode score around the time of implantation is predictive of successful implantation following frozen embryo transfer in hormone replacement cycles. *Hum Reprod*. 2017;32:2394–2403. doi:10.1093/humrep/dex312
10. Aunapuu M, Kibur P, Järveots T, et al. Changes in morphology and presence of pinopodes in endometrial cells during the luteal phase in women with infertility problems: a Pilot Study. *Medicina*. 2018;54(5):69. doi:10.3390/medicina54050069
11. Psychoyos A, Mandon P. Study of the surface of the uterine epithelium by scanning electron microscope. Observa-tions in the rat at the 4th and 5th day of pregnancy. *CR Acad Sci Hebd Seances Acad Sci D*. 1971;272:2723–2725.
12. Singh MM, Chauhan SC, Trivedi RN, et al. Correlation of pinopod development on uterine luminal epithelial surface with hormonal events and endometrial sensitivity in rat. *Eur J Endocrinol*. 1996;135:107–117. doi:10.1530/eje.0.1350107
13. Massimiani M, Lacconi V, La Civita F, et al. Molecular signaling regulating endometrium–blastocyst crosstalk. *Int J Mol Sci*. 2019;21:23. doi:10.3390/ijms21010023
14. Gambino LS, Wreford NG, Bertram JF, et al. Angiogenesis occurs by vessel elongation in proliferative phase human endometrium. *Hum Reprod*. 2002;17:1199–1206. doi:10.1093/humrep/17.5.1199
15. Yang X, Gilman-Sachs A, Kwak-Kim J. Ovarian and endometrial immunity during the ovarian cycle. *J Reprod Immunol*. 2019;133:7–14. doi:10.1016/j.jri.2019.04.001
16. Tan Q, Shi S, Liang J, et al. Endometrial cell-derived small extracellular vesicle miR-100-5p promotes functions of trophoblast during embryo implantation. *Mol Ther Nucleic Acids*. 2021;23:217–231. doi:10.1016/j.omtn.2020.10.043
17. Torry DS, Leavenworth J, Chang M, et al. Angiogenesis in implantation. *J Assist Reprod Genet*. 2007;24:303–315. doi:10.1007/s10815-007-9152-7
18. Li S, Ding L. Endometrial perivascular progenitor cells and uterus regeneration. *J Pers Med*. 2021;11(6):477. doi:10.3390/jpm11060477
19. Li M, Hu J, Yao L, et al. Decreased ANGPTL4 impairs endometrial angiogenesis during peri-implantation period in patients with recurrent implantation failure. *J Cell Mol Med*. 2020;24(18):10730–10743. doi:10.1111/jcmm.15696
20. Zhang S, Kong S, Lu J, et al. Deciphering the molecular basis of uterine receptivity. *Mol Reprod Dev*. 2013;80:8–21. doi:10.1002/mrd.22118
21. Wang T, Kang X, Zhao A, et al. Low-dose aspirin improves endometrial receptivity in the midluteal phase in unexplained recurrent pregnancy loss. *Int J Gynaecol Obstet*. 2020;150(1):77–82. doi:10.1002/ijgo.13160
22. Casper RF. Frozen embryo transfer: evidence-based markers for successful endometrial preparation. *Fertil Steril*. 2020;113:248–251. doi:10.1016/j.fertnstert.2019.12.008
23. Liu H, Zhang J, Wang B, et al. Effect of endometrial thickness on ectopic pregnancy in frozen embryo transfer cycles: an analysis including 17,244 pregnancy cycles. *Fertil Steril*. 2020;113:131–139. doi:10.1016/j.fertnstert.2019.09.003
24. Coelho Neto MA, Martins WP, Lima MLS, et al. Ovarian response is a better predictor of clinical pregnancy rate following embryo transfer than is thin endometrium or presence of an endometrioma. *Ultrasound Obstet Gynecol*. 2015;46:501–505. doi:10.1002/uog.14884

25. Chen M, He Y, Zhang P, et al. Comparison of uterine receptivity between fertile and unexplained infertile women by assessment of endometrial and subendometrial perfusion using contrast-enhanced ultrasound: which index is better–peak intensity or area under the curve? *Ultrasound Med Biol*. 2016;42:654–663. doi:10.1016/j.ultrasmedbio.2015.11.008

26. Frinking P, Segers T, Luan Y, et al. Three decades of ultrasound contrast agents: a review of the past, present and future improvements. *Ultrasound Med Biol*. 2020;46:892–908. doi:10.1016/j.ultrasmedbio.2019.12.008

27. Güvener N, Appold L, de Lorenzi F, et al. Recent advances in ultrasound-based diagnosis and therapy with micro- and nanometer-sized formulations. *Methods*. 2017;130:4–13. doi:10.1016/j.ymeth.2017.05.018

28. Yan F, Wu H, Liu H, et al. Molecular imaging-guided photothermal/photodynamic therapy against tumor by iRGD-modified indocyanine green nanoparticles. *J Control Release*. 2016;224:217–228. doi:10.1016/j.jconrel.2015.12.050

29. Cheow WS, Hadinoto K. Factors affecting drug encapsulation and stability of lipid-polymer hybrid nanoparticles. *Colloids Surf B Biointerfaces*. 2011;85:214–220. doi:10.1016/j.colsurfb.2011.02.033

30. Huang W, Xin W, Xiang G, et al. Maleimide-thiol adducts stabilized through stretching. *Nat Chem*. 2019;11:310–319. doi:10.1038/s41557-018-0209-2

31. Valdes CT, Schutt A, Simon C. Implantation failure of endometrial origin: it is not pathology, but our failure to synchronize the developing embryo with a receptive endometrium. *Fertil Steril*. 2017;108:15–18. doi:10.1016/j.fertnstert.2017.05.033

32. Karizbodagh MP, Rashidi B, Sahebkar A, et al. Implantation window and angiogenesis. *J Cell Biochem*. 2017;118:4141–4151. doi:10.1002/jcb.26088

33. Koot YE, Van Hooff SR, Boomsma CM, et al. An endometrial gene expression signature accurately predicts recurrent implantation failure after IVF. *Sci Rep*. 2016;6:19411. doi:10.1038/srep19411

34. Demir R, Yaba A, Huppertz B. Vasculogenesis and angiogenesis in the endometrium during menstrual cycle and implantation. *Acta Histochem*. 2010;112:203–214. doi:10.1016/j.acthis.2009.04.004

35. Chen X, Man GCW, Liu Y, et al. Physiological and pathological angiogenesis in endometrium at the time of embryo implantation. *Am J Reprod Immunol*. 2017;78:e12693. doi:10.1111/aji.12693

36. Chen Y, Liang Y, Jiang P, et al. Lipid/PLGA hybrid microbubbles as a versatile platform for noninvasive image-guided targeted drug delivery. *ACS Appl Mater Interfaces*. 2019;11:41842–41852. doi:10.1021/acsami.9b10188

37. Liu X, Lin P, Perrett I, et al. Tumor-penetrating peptide enhances transcytosis of silicasome-based chemotherapy for pancreatic cancer. *J Clin Invest*. 2017;127:2007–2018. doi:10.1172/JCI92284

38. Wang S, Guo X, Ren L, et al. Targeting and deep-penetrating delivery strategy for stented coronary artery by magnetic guidance and ultrasound stimulation. *Ultrason Sonochem*. 2020;67:105188. doi:10.1016/j.ultsonch.2020.105188

39. Fan CH, Cheng YH, Chien-Yu T, et al. Ultrasound/magnetic targeting with SPIO-DOX-microbubble complex for image-guided drug delivery in brain tumors. *Theranostics*. 2016;6:1542–1556. doi:10.7150/thno.15297